Journal of Alloys and Compounds 513 (2012) 230–235

Contents lists available at SciVerse ScienceDirect

Journal of Alloys and Compounds

journal homepage: www.elsevier.com/locate/jallcom

Structural characteristics of quantum-size ceria nano particles synthesized via simple ammonia precipitation

Neeroli Kizhakayil Renuka*

Department of Chemistry, University of Calicut, Kerala 673 635, India

ARTICLE INFO

Article history:
Received 23 August 2011
Received in revised form 8 October 2011
Accepted 11 October 2011
Available online 18 October 2011

Keywords:
Nanostructured material
Ceria
Precipitation
TEM
XPS

ABSTRACT

Nanoscale, high surface area spherical cerium oxide was prepared from aqueous cerium nitrate by homogeneous precipitation using ammonia. This synthesis route offers a versatile, low cost and environmental friendly method to produce nano ceria. The specimen powder was characterized with XRD, SEM, HRTEM, and UV–vis spectrophotometry. Cubic cerianite crystallites (CeO_2) were detected by powder XRD pattern, while Ce^{3+} was also evident from XPS spectra and DR UV spectroscopy study. XPS spectra indicated that cerium in the nano crystals was predominantly tetravalent. Both Ce_2O_3 as well as oxygen vacancy contributed towards the presence of Ce^{3+} in the sample. The particle size of the system was calculated from TEM analysis, XRD study and BET surface area analysis. The characterization revealed the particles to be spherical in shape with typical size 4–5 nm, which is a favourable characteristic feature for many applications. The direct optical band gap estimated from DR UV absorption spectrum was blue-shifted evidently with respect to the bulk material and indicated quantum-size confinement effect in nano crystallites.

1. Introduction

Nanoparticles have received much attention in the field of material science because of their fascinating mechanical and physico-chemical properties which are entirely different from their bulk counterparts. Among nanoparticles, semiconductor nanocrystals with tunability of electronic and optical properties have attracted considerable interest. Cerium (IV) oxide (CeO_2, cerianite), with a cubic fluorite-type structure is one among those, which finds versatile applications in various fields, including solid-state physics, chemistry, and material science. The flexibility of band gap in nano ceria makes them proper objects for various applications such as the Raman-allowed modes shifting and broadening [1] and lattice expansion [2]. They are also being used to probe fundamental material properties such as magnetic/electronic interactions [3]. The ability of cerium oxide to reversibly exchange oxygen is a key aspect of the material that helps to act as oxygen buffer through redox processes involving the Ce^{4+}/Ce^{3+} couple. Due to this feature, ceria is widely used as promoter, and support in many catalytic processes. The role of ceria nanoparticles and their mixed analogues in catalyzing oxidation reactions of industrial and environmental significance has been extensively studied owing to this fine property [4–8]. Nano ceria supported metal catalysts were also investigated by different groups [9,10]. The promoting effect of the oxide in these cases was attributed to the boosting of oxygen transfer to the reaction site [11]. Apart from this, studies are also initiated to pursue the photocatalytic activity of nano ceria [12]. The material was also proposed for biomedical applications. It has been reported that the introduction of trace amounts of ceria into retina notably reduces the adverse effect of UV radiation on photoreceptor cells of the eye [13]. Another interesting application of the material is its biocompatibility for applications in diseases of the central nervous system as reported by Das et al. [14]. Very recently, ecotoxicological assessment of CeO_2 nanoparticles has been studied by Rodea Palomers et al. [15]. Other latest advances in this area include search for novel synthetic strategies for achieving nanoparticles of ceria with desirable properties, and their surface modifications [16–19]. In the present work, we report a simple homogeneous ammonia precipitation method to obtain cerium oxide nano crystals which have optimum size for many applications, from aqueous cerium nitrate solution. Methods that are reported earlier demands micro emulsion technique, presence of hydrogen peroxide, etc., and hence, this synthetic route is an adaptable, cost effective and environmental friendly one. The prepared oxide was characterized using X-ray diffraction (XRD), scanning electron microscopy (SEM), nitrogen adsorption study, UV–vis DRS, transmission electron microscopy (TEM) and X-ray photoelectron spectroscopy (XPS). The crystalline phase, surface morphology, microstructure, porosity characteristics, particle size, band gap energy, etc. are discussed in detail. The presence of different oxidation states of cerium, and their mode of

* Corresponding author. Tel.: +91 494 2401144x414; fax: +91 494 2400269.
E-mail address: nkrenu@gmail.com

0925-8388/$ – see front matter © 2011 Elsevier B.V. All rights reserved.
doi:10.1016/j.jallcom.2011.10.027

existence in the oxide are substantiated by the results derived from XPS analysis.

2. Experimental

2.1. Synthesis of ceria

All chemicals were purchased from Aldrich (Germany), purity 99.99%. CeO_2 nanoparticles were prepared by a process that involves the homogeneous precipitation of a solution of cerium nitrate hexahydrate ($Ce(NO_3)_3{\cdot}6H_2O$) with dilute aqueous ammonia. The methodology adopted was a slight modified version of the one reported by Zhou et al. [20]. The requisite quantity of precursor was dissolved in double distilled water and was precipitated by drop wise addition of the solution to aqueous ammonia over a period. Excess precipitant was maintained during the process. The obtained light yellow coloured slurry was washed 10 times with deionised water to remove any water-soluble species and subsequently washed 3 times with ethanol to remove water and disrupt hydrogen bonded networks between water and the precursor, which otherwise led to severe aggregation upon heating. The collected precipitate was oven-dried at 383 K for 12 h, crushed using an agate mortar, and subsequently calcined at 500 °C for 3 h in air atmosphere to obtain the oxide material.

2.2. Characterization of cerium oxide particles

The nano powder was characterized by adopting following methodologies. Powder X-ray diffraction (XRD) pattern results of the samples were collected on a Rigaku D/MAX- diffractometer equipped with a rotating anode using Cu$K\alpha$ radiation. Scherrer equation was applied to the maximum intense peak in order to determine the crystallite size of the particles. Brucker Nanostar instrument was used to obtain low angle XRD diffraction pattern. The micro structure of the samples was obtained by transmission electron microscopic (TEM) images with a Philips CM 200 transmission electron microscope operating at 20–200 kV range. Sample grids were prepared by sonicating powdered samples in ethanol for 20 min and evaporating one drop of the suspension onto a carbon-coated, holey film supported on a 3-mm, 300-mesh copper grid. Scanning electron microscopic (SEM) images were recorded using a SEM – JSM 848 instrument. N_2 adsorption–desorption isotherms were obtained on a Micromeritics Gemini Surface Area analyzer using a static adsorption procedure at 77 K. Samples were degassed at 150 °C in a vacuum below 10^{-3} Torr for 16 h prior to the measurements. The specific surface area was calculated using the BET equation for data in a (P/P_0) range between 0.05 and 0.3. The pore-size distributions were calculated from the data of the desorption branch of the isotherm using the Barrett– Joyner–Halenda (BJH) method. DR UV–vis spectra were taken in the range 200–800 nm with $BaSO_4$ as reference using Jasco V-550 spectrophotometer. X-ray photoelectron spectroscopic (XPS) measurements were carried out on a VG Micro Tech ESCA 300° instrument at a pressure of $>1 \times 10^{-9}$ Torr (pass energy of 50 eV, electron take off angle 60° and the overall resolution was ~0.1 eV).

3. Results and discussion

Interesting changes appeared in colour of the solution when cerium nitrate solution was added to the precipitant. Initially, at low pH, the slurry was purple, possibly due to Ce^{3+}, which finally changed to yellow colour due to the formation of Ce^{4+} in the presence of oxygen. The synthesized particles were subjected to different characterization methods to yield the following results.

3.1. XRD analysis

Fig. 1 shows the wide angle powder X-ray diffraction pattern of cerium oxide powder. The as-prepared sample exhibited rather amorphous character as indicated by the diffraction pattern. Their broad, indistinct feature suggests that the material is either amorphous or of a crystal size too small for this method to resolve. The peaks sharpened as the treatment temperature increased to 500 °C. All Bragg peaks with Miller indices (1 1 1), (2 0 0), (2 2 0), (3 1 1), (2 2 2), (4 0 0), (3 3 1) and (4 2 0) were associated with the cubic lattice of pure CeO_2 (CaF_2 structural type), and was in good agreement with literature data (JCPDS No. 34-0394). No identifiable diffraction peaks of crystalline Ce_2O_3 phase was noticed in the XRD pattern of these nano particles. The lattice constant of the cubic fluorite-type CeO_2 grains can be determined through the spacing of the lattice planes, which was observed to be ~0.54 nm, with space group $Fm3m$. The mean grain size of CeO_2 was determined from the broadening full width at half maximum$_{hkl}$ (FWHM)$_{hkl}$ of the XRD peaks,

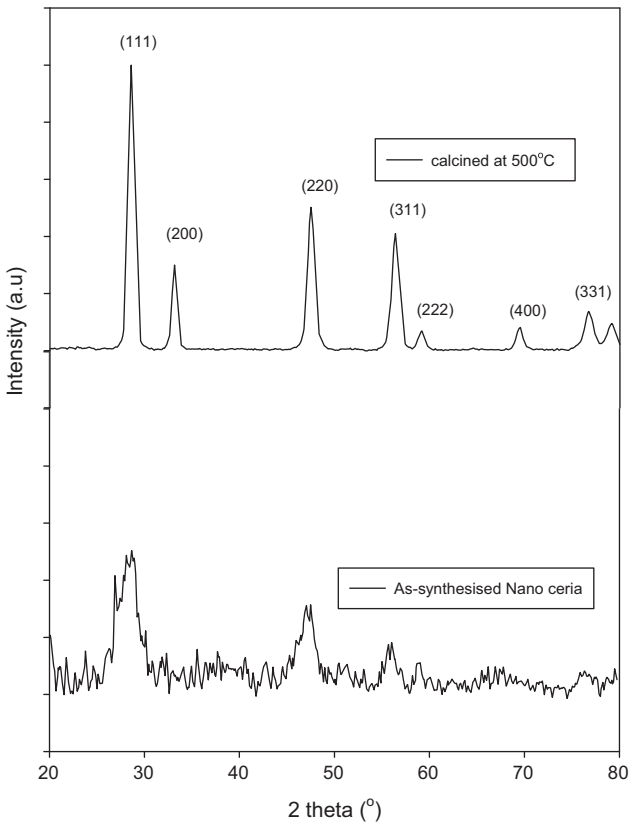

Fig. 1. Wide angle powder XRD pattern of cerium oxides.

which correspond to the lattice planes with Miller indices ($h\,k\,l$), through Scherrer's formula. The XRD pattern of the as-synthesized material yielded the crystallite size of cerium oxide nanoparticles to be 4.6 nm, which upon calcination increased to 4.9 nm, showing agglomeration of primary particles perhaps may be due to sintering. The influence of particle size on lattice parameter do exists in particles. It was noticed that, as the particle size decreases, the value of lattice parameter increases. For bulk material, the lattice parameter is 0.5410 nm, and fabricating into nano size decreased the value as shown in Table 1. The decrease in lattice parameter of the particle upon heat treatment is also clear from the table.

3.2. Scanning electron microscopy (SEM) analysis

Morphology of the cerium oxide powder sample is examined using scanning electron microscopy. The SEM micrograph of the as prepared ceria powder illustrated in Fig. 2. On close observation, rather agglomerated uniform spherical grains of average size below 10 nm were identified.

3.3. Transmission electron microscopy (TEM) analysis

The TEM image in Fig. 3(a) illustrates aggregated primary crystallites with typical size of 4–5 nm in the as-synthesized sample, which agrees well with SEM pattern. The mean size is consistent with the XRD particle size estimation using the full width at half-maximum and Scherrer formula (Table 1). The selected area electron diffraction (SAED) pattern provided in inset justifies the amorphous form of nano ceria, as indicated by powder XRD pattern. The HRTEM image of calcined ceria is provided in Fig. 3(b), which confirms the dimension of the crystallites. The size of the prepared nano particles is suitable for many applications including biomedical applications [14]. When the as prepared ceria was

Table 1
Physical characterization data of nano ceria.

Ceria	Average particle size (nm)			Lattice parameter (nm)	Surface area (m^2/g)	Average pore diameter (nm)	Pore volume (cm^3/g)
	XRD	TEM	BET				
As-prepared	4.6	4.8	(9.01)	0.5419	113.3	3.72	0.088
Calcined ceria	4.9	5.1	(14.01)	0.5412	93.01	4.91	0.030

calcined at 550 °C, the crystalline nature increased, as evident from the electron diffraction pattern, which assigns the cubic phase for the material (Fig. 3(b)). Obviously, this observation is also consistent with the result of XRD. The (1 1 1) phase of the oxide particle is quite clear in the TEM pattern. Cerium oxide has a cubic fluorite structure, both in bulk and nanoparticle forms. The low index exposed crystal planes have been shown to have differing reactivity [21]. The {1 1 1} surface plane is the most stable, followed by the {1 1 0} and {1 0 0} planes. The formation of an oxygen vacancy occurs more easily for the {1 1 0} surfaces than in the {1 1 1} surfaces. The vacancies tend to form in the surface layer for {1 1 0} whereas for the {1 1 1} surface they tend to form in the subsurface layer [22].

3.4. N_2 adsorption studies

Fig. 4 displays N_2 adsorption–desorption isotherms and the corresponding pore size distributions of the heat treated sample. The isotherm can be ascribed to type IV belonging to H3 group implying the presence of typical conterminous textural porosity. Textural porosity arises from non-crystalline intra aggregate voids and spaces formed by inter particle contacts. The values of surface area and other porosity parameters are provided in Table 1. It is well-known that ceria shows high oxidation ability due to its high oxygen vacancies and a low redox potential between Ce^{3+} and Ce^{4+}. Possibly due to that, surface areas and the concentration of the defects (such as oxygen vacancies) were remarkably increased when the particle size was decreased to nanometer scale. The surface area value obtained for the system was rather very high considering the fact that the synthetic route is template free, and the value got reduced when heat treated, as expected (Table 1). Recently, studies have demonstrated that the BET method can be used to obtain average particle diameter assuming nonporous spherical/cubical nano particles and a theoretical density of the individual materials. Without going through the entire derivation, the equation for calculating the average particle diameter in nanometers is 6000/(BET surface area in $m^2/g \times$ density in g/cm^3). The equation will vary slightly for other uniformly shaped materials. The average particle size of ceria (true density 7.13 g/cm^3) derived from this equation is presented in Table 1, which shows the deviation of the said values from those obtained from TEM. The above mentioned method led to surface area values higher than those obtained from TEM analysis. The difference observed between the two values is due to the fact that a small amount of surface is being lost due to the primary particles forming aggregates. It is clear that the discrepancy between the values obtained from these two methods is more in the case of calcined ceria, where more aggregates are expected.

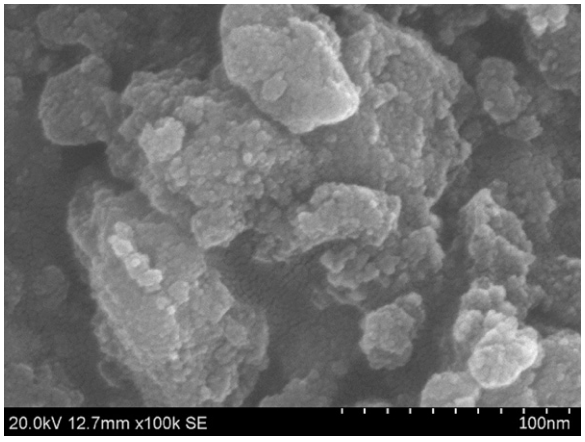

Fig. 2. SEM photograph showing morphology of the ceria powder.

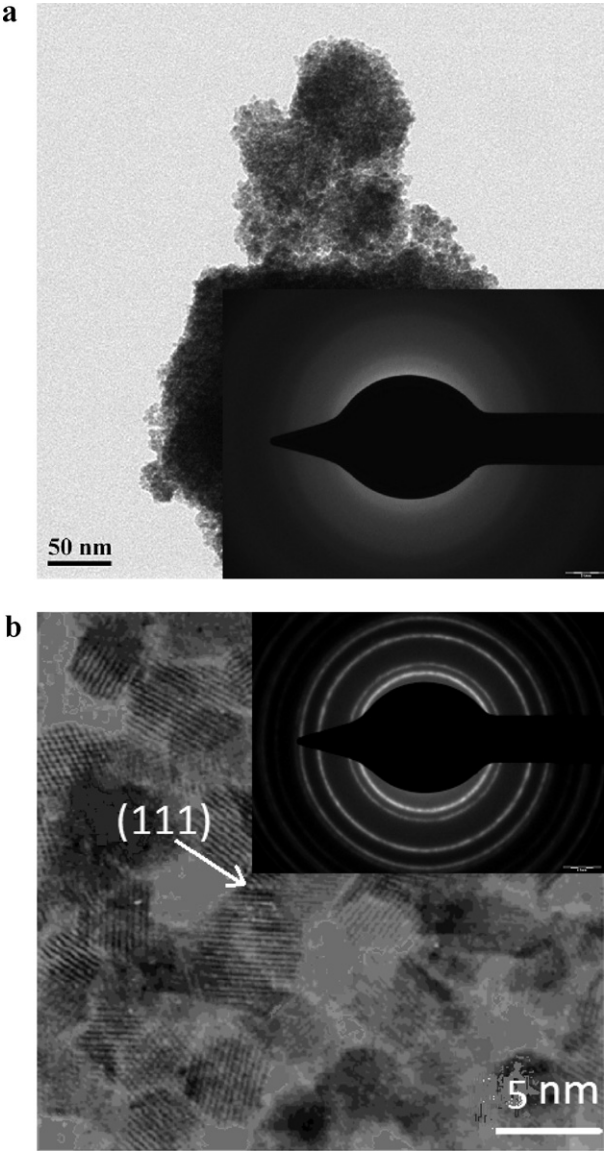

Fig. 3. (a) TEM image of as-prepared ceria particles showing particle size and SAED pattern (inset). (b) HRTEM image of ceria calcined at 500 °C. SAED pattern (inset).

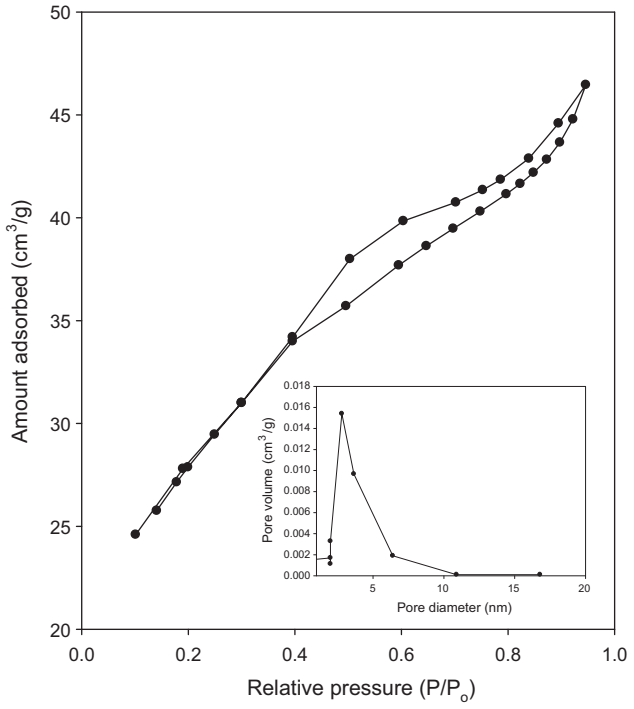

Fig. 4. N_2 adsorption isotherm of calcined ceria. Pore size distribution profile (inset).

3.5. Diffuse reflectance UV spectral analysis

The UV–vis absorption spectra of the nano CeO_2 obtained in the present study is presented in Fig. 5. The diffuse reflectance spectra of bulk ceria (Sigma–Aldrich, 99.9% trace metal basis) is also provided for comparison. The spectra show that both of the samples have intense absorption in the UV that trails into the visible region of the spectrum. Generally, the absorption of ceria in the UV region originated from charge-transfer transition between O2p and Ce4f bonds, which overruns the well-known f to f spin–orbit

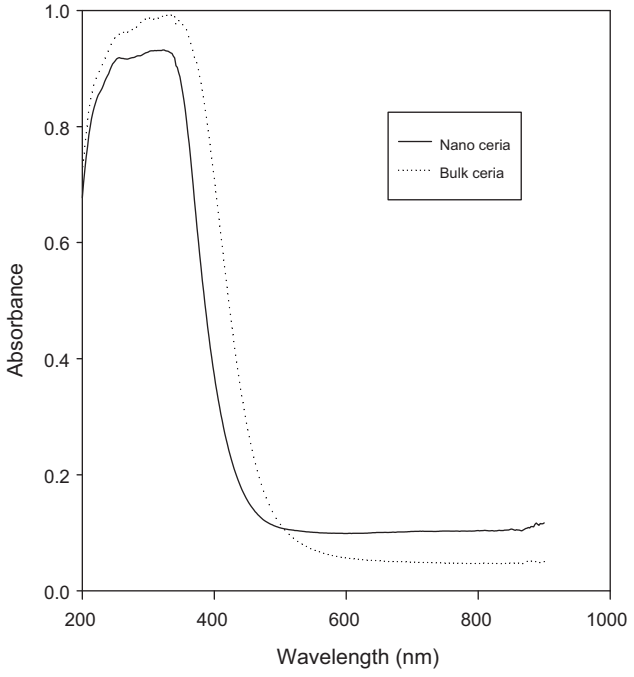

Fig. 5. Diffuse reflectance pattern of ceria samples.

Table 2
Binding energy associated with different peaks of cerium ions.

Peak	Binding energy (eV)	Cerium state
*v*o	880.59	3+
v	882.77	4+
v′	885.60	3+
v″	889.06	4+
v‴	898.02	4+
*u*o	899.03	3+
u	902.03	4+
u′	905.23	3+
u″	908.13	4+
u‴	917.42	4+

splitting of the Ce 4f state [23,24]. The UV-DR spectrum on curve splitting exhibited two prominent peaks, one at 250 nm and the other one around 315 nm and a comparatively small one at 280 nm. The first peak corresponds to Ce^{3+} variety present which is caused by $Ce^{3+} \leftarrow O^{2-}$ in the system, though XRD ruled out the possibility of the Ce^{3+} species. The second peak arises due to inter band transition in ceria, and the weak band at 280 nm is assigned to $Ce^{4+} \leftarrow O^{2-}$ charge transfer transitions [25–28].

The wavelength corresponding to the UV absorption edge of a semiconducting powder such as CeO_2 can be safely used to probe the presence of nano-crystallites (~5 nm). The absorption edge of nano CeO_2 is blue-shifted compared to that of the bulk material. The blue shifting in the UV absorption spectra of CeO_2 nano crystals has attracted much interest of many researchers in recent years [29–32]. The blue shift of the absorbance and subsequent increase of band gap of nano sized particles of ceria result from the small crystal size [33]. It was theoretically deduced that the value of blue-shifting resulting from the reduction of particle size is inversely proportional to the square of the size due to quantum confinement effect. Since the typical size of the nano crystals (4–5 nm) is far smaller than 2*a*B, where *a*B is the exciton Bohr radius of the material (about 7–8 nm) [34], the optical band gap shift should be classified to strong confinement regime [35]. Thus, a decrease in the nano crystal size should be accompanied by an increase of the effective width of the forbidden band E_g, the energy difference between the lower energy of conduction band and the upper energy of valence band. As a result, the absorption band is shifted to the range of higher energy and blue-shift is observed [36]. In the present study, the optical band gap E_g was calculated based on the absorbance spectrum of the powders, using equation, $E_{BG} = 1240/\lambda_{Absorp.Edge}$ [37]. The onset of absorption of nano and bulk CeO_2 were at ~440 and 410 nm, which corresponds to the band gap energy of ca. 2.81 and 3.02 eV, respectively. These values are consistent with the characteristic values given in literature for CeO_2 materials.

3.6. X-ray photo electron spectroscopy

XPS peaks enable to identify binding energy and associated oxidation states of cerium in the oxide sample. Fig. 6(b) shows the individual peaks of Ce3d pattern after deconvolution. Ten peaks are identified, six corresponding to Ce^{4+} state and four representing Ce^{3+} state [38]. The binding energy values for different peaks corresponding to each ion are presented in Table 2. Two sets of spin–orbital multiplets, corresponding to the $3d_{3/2}$ and $3d_{5/2}$ contributions were labeled as *u* and *v*, respectively. Peaks *u*‴ (917.42 eV) and *v*‴ (898.02 eV) originate from Ce $3d^9$ $O2p^6$ Ce $4f^0$ final states of Ce^{4+}. The additional states of Ce^{4+}, [*u* (902.3 eV), *v* (882.7 eV), *u*″ (908.13 eV), *v*″ (889.06 eV)] result from a mixture of Ce $3d^9$ O $2p^5$ Ce $4f^1$ and Ce $3d^9$ O $2p^4$ Ce $4f^2$ final states. Finally, the contribution of Ce^{3+} to the Ce3d spectrum consists of two doublet pairs: (i) *u*′ (~905.23 eV), *v*′ (885.6 eV) and (ii) *uo* (899.03 eV), *vo*

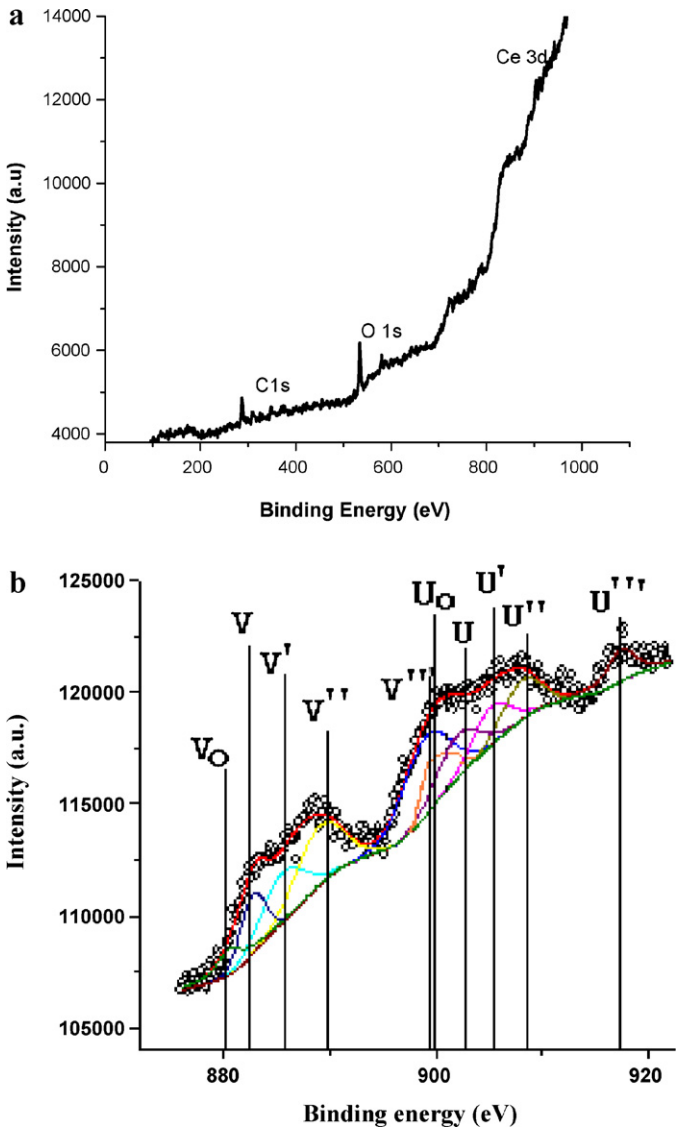

Fig. 6. (a) XPS spectra of ceria—survey spectra. (b) XPS spectra—Ce 3d peaks.

(880.3 eV). These doublets correspond to a mixture of the Ce $3d^9$ $O2p^5$ Ce $4f^2$ and Ce 3d9 O2p6 Ce $4f^1$ final states.

The sum of peak area corresponding to the ions is proportional to the concentration of ions. Hence concentration of two oxidation states in the oxide sample can be obtained by the expression given below [39].

$Ce^{3+} = vo + v' + uo + u'$; $Ce^{4+} = v + v'' + v''' + u + u'' + u'''$ and hence

$$[Ce^{3+}] = \frac{Ce^{3+}}{Ce^{3+} + Ce^{4+}} \quad \text{and} \quad [Ce^{4+}] = \frac{Ce^{4+}}{Ce^{3+} + Ce^{4+}}$$

The calculations led to the fact that in these ceria nano particles, 67% of cerium is present in the tetravalent state, while the remaining 33% exist as trivalent ion. Thus XPS also reveal the existence of a considerable amount of Ce^{3+} in the system, although XRD identified only the tetravalent cerium as CeO_2. The trivalent Ce^{3+} can be distributed either in regions of sesquioxide Ce_2O_3 or around O vacancies in CeO_2 [40]. This observation has been well established in previous reports. Further investigation on the presence of Ce^{3+}, i.e., whether due to Ce_2O_3 or due to O vacancies, O content is calculated assuming that the total O content is the sum of the required O to fully oxidize Ce^{4+} and Ce^{3+} into respective oxides. That is assuming that Ce^{3+} and Ce^{4+} exclusively form Ce_2O_3 and CeO_2, respectively. The required O to fully oxidize the whole cerium ions (the parameter 'x' in the stoichiometric formula CeO_x) is determined using the formula,

$$x = \frac{[O]}{[Ce]} = \frac{3}{2}[Ce^{3+}] + 2[Ce^{4+}]$$

considering the fact that $x = [O]/[Ce]$ is equal to 2 for CeO_2 and 1.5 for Ce_2O_3. Here $[Ce] = [Ce^{3+}] + [Ce^{4+}]$, that can be derived from XPS analysis. The stoichiometry of oxygen was obtained to be 1.84 per Ce atom. The stoichiometry was cross checked with the direct O to Ce ratio derived from the intensity of corresponding peaks in XPS spectra, which was observed to be slightly different (1.78), indicating that oxygen vacancy also contributes to the presence of Ce^{3+} in these particles. It has been reported that the oxygen vacancies exist more in systems with higher $[Ce^{3+}]$. Alternatively, the small particle size leads to higher oxygen vacancy which in turn explains the higher concentration of Ce^{3+} in nano systems. The reduction of CeO_2 to $CeO_{2-\gamma}$ ($\gamma = 2 - x$) is caused by the oxygen atoms vacating the crystal lattice, which lead to reduction of adjacent Ce(IV) ions to Ce(III). These oxygen vacancies that form, leaving oxygen depleted Ce(III) ion behind, are responsible for the high reactivity in nano ceria.

4. Conclusions

The template free precipitation of ceria from cerium nitrate hexahydrate by ammonia resulted in nano sized particles with spherical morphology. Cubic CeO_2 crystallites were detected by powder XRD pattern, while the presence of negligible amount of trivalent Ce^{3+} was also evident from XPS spectra and DR UV spectroscopy study. The percentage composition of Ce^{4+} was obtained to be 67. Both Ce_2O_3 as well as oxygen vacancy contributed towards the presence of Ce^{3+} in the sample. The characterization revealed the particles to be of typical size between 4 and 5 nm. The direct optical band gap estimated from ultraviolet absorption spectrum of the nano ceria is blue-shifted evidently with respect to the bulk material and indicated quantum-size confinement effect in nano crystallites. The synthesized ceria has dimensions suitable for many applications including biomedical applications.

Acknowledgement

The financial assistance received from Kerala State Council for Science Technology and Environment is gratefully acknowledged.

References

[1] W.H. Weber, K.C. Hass, J.R. Mc Bride, Phys. Rev. B 48 (1993) 178–185.
[2] X.D. Zhou, W. Huebner, Appl. Phys. Lett. 79 (2001) 3512–3515.
[3] A. Schroder, G. Aeppli, R. Coldea, M. Adams, O. Stockert, H.V. Lohneysen, E. Bucher, R. Ramazashvili, P. Coleman, Nature 407 (2000) 351–355.
[4] N.G. Hurtado, I. Atribak, A.B. Lopez, A.G. García, J. Mol. Catal. A: Chem. 323 (2010) 52–58.
[5] M. Cargnello, C. Gentilini, T. Montini, E. Fonda, S. Mehraeen, M. Chi, X.M.H. Collado, N.D. Browning, S. Polizzi, O.L. Pasquato, P. Fornasiero, Chem. Mater. 22 (2010) 4335–4345.
[6] Y. Liu, C. Wen, Y. Guo, G. Lu, Y. Wang, J. Phys. Chem. C 114 (2010) 9889–9897.
[7] R. Wang, P.A. Crozier, R. Sharma, J. Phys. Chem. C 113 (2009) 5700–5704.
[8] M. Benjaram, L. Reddy, G. Katta, Thrimurthulu, Chem. Mater. 22 (2010) 467–475.
[9] J.F. Bozeman III, H. Huang, J. Nanomater. (2011) 6, doi:10.1155/2011/329757, Article ID: 329757.
[10] J.A. Farmor, C.T. Campbell, Science 329 (5994) (2010) 933–936.
[11] G.N. Vayssilov, Y. Lykhach, A. Miani, T. Staudt, G.P. Petrova, N. Tsud, T. Skala, A. Bruix, F. Illas, K.C. Prince, J. Libuda, Nat. Mater. 10 (2011) 310–315.
[12] H.R. Pouretedal, A. Kadkhodaie, Chin. J. Catal. 31 (11) (2010) 1328–1334.
[13] J. Chen, S. Patil, S. Seal, J.F. Ginnis, Nat. Nanotechnol. 1 (2006) 142–150.
[14] M. Das, S. Patil, N. Bhargava, J.F. Kang, L.M. Riedel, S. Seal, J.J. Hickman, Biomaterials 28 (2007) 1918–1925.
[15] I.R. Plaomers, K. Bolts, F.F. Pinas, F. Leganza, E.G. Carvo, J. Santiago, R. Rosal, Toxicol. Sci. 119 (1) (2011) 135–145.

[16] V.K. Ivanov, O.S. Polezhaeva, A.S. Shaporev, A.E. Baranchikova, A.B. Shcherbakov, A.V. Usatenko, Russ. J. Inorg. Chem. 55 (3) (2010) 328–332.
[17] Q.C. Zhang, Z.H. Yu, G. Li, Q.M. Ye, J.H. Lin, J. Alloys Compd. 477 (2009) 81–84.
[18] D. Valechha, S. Lokhande, M. Klementova, J. Subrt, S. Rayalua, N. Labhsetwar, J. Mater. Chem. 21 (2011) 3718.
[19] J. Zhang, T. Naka, S. Ohara, K. Kaneko, T. Trevethan, A. Shulger, T. Adschiri, Phys. Rev. B 84 (2011) 045411–045420.
[20] X.D. Zhou, W. Huebner, H.U. Anderson, Chem. Mater. 15 (2003) 378–382.
[21] K. Zhou, X. Wang, X. Sun, Q. Peng, Y. Li, J. Catal. 229 (2005) 206–212.
[22] Z.X. Yang, T.K. Woo, M. Baudin, K. Hermansson, J. Chem. Phys. 120 (2004) 7741–7747.
[23] S. Tsunekawa, T.J. Fukuda, J. Appl. Phys. 87 (1999) 1318–1321.
[24] S. Tsunekawa, R. Sahara, Y. Kawazoe, A. Kasuya, Mater. Trans. JIM 41 (2000) 1104–1107.
[25] G. Ranga Rao, H. Ranjan Sahu, Proc. Indian Acad. Sci. (Chem. Sci.) 113 (October–December (5–6)) (2001) 651–658.
[26] A. Martinez-Arias, M. Fernandez-Garcıa, L.N. Salamanca, R.X. Valenzuela, J.C. Conesa, J. Soria, J. Phys. Chem. B 104 (2000) 4038–4046.
[27] M.I. Zaki, G.A.M. Hussein, S.A.A. Manssur, H.M. Ismael, G.A.H. Mekhemer, Colloids Surf. A 127 (1997) 47–56.
[28] A. Bensalem, J.C. Muller, F. Bozon-Verduraz, J. Chem. Soc. Faraday Trans. 88 (1992) 153–154.
[29] T. Masui, K. Fujiwara, K.I. Machida, G.Y. Adachi, Chem. Mater. 9 (1997) 2197–2204.
[30] M. Inoue, M. Kimura, T. Inui, Chem. Commun. 11 (1999) 957–958.
[31] L.X. Yin, Y.Q. Wang, G.S. Pang, Y. Koltypin, A. Gedanken, J. Colloid Interface Sci. 246 (2002) 78–84.
[32] H. Wang, J.J. Zhu, J.M. Zhu, X.H. Liao, S. Xu, T. Ding, H.Y. Chen, Phys. Chem. Chem. Phys. 4 (2002) 3794–3799.
[33] S. Tsunekawa, T. Fukuda, A. Kasuya, J. Appl. Phys. 87 (2000) 1318–1321.
[34] S. Tsunekawa, J.T. Wang, Y. Kawazoe, A. Kasuya, J. Appl. Phys. 94 (2003) 3654–3656.
[35] S.S. Nair, M. Mathews, M.R. Anantharaman, Chem. Phys. Lett. 406 (2005) 398–403.
[36] A.I. Gusev, A.A. Rempel, Nanocrystalline Materials, Cambridge Inter. Sci., Cambridge/London, 2004.
[37] P. Ji, J. Zhang, F. Chen, M. Anpo, J. Phys. Chem. C 112 (46) (2008) 17809–17813.
[38] P. Patsalas, S. Logothetidis, Phys. Rev. B 68 (2003) 035104.
[39] J. Zhang, X. Ju, Z.Y. Wu, T. Liu, T.D. Hu, Y.N. Xie, Z.L. Zhang, Chem. Mater. 13 (2001) 4192–4197.
[40] F. Marabelli, P. Wachter, Phys. Rev. B 36 (1987) 1238–1245.